Bulletin of the Seismological Society of America, Vol. 88, No. 3, pp. 744–757, June 1998

Spectral Structure in the Earth's Microseismic Background between 20 and 40 Seconds

by L. Gary Holcomb

Abstract The long-term behavior of a narrow band peak near 26 sec in the microseismic background of the Earth has been studied over many years at several sites. The amplitude of this peak has been determined to be a function of the Earth's weather seasons; it is larger during the southern hemisphere winter. In addition, the microseismic background between 20 and 40 sec has been scanned for peaks in the spectra; three more lower-level peaks have been identified with the possible presence of more.

Introduction

The ambient background Earth motion is the ultimate limiting factor in determining the lower levels for detecting seismic events at a given site. The background noise levels in parts of the spectrum are frequently dominated by local sources such as cultural noise created by motor vehicle vibrations, railroad noise, heavy equipment operating in factories and construction projects, mining activity, etc. Therefore, seismic installations are usually placed as far from potential cultural noise sources as feasible to reduce their contribution to the seismic background. Local wind-generated ground motion also contributes to the site background; therefore, seismic sensors are frequently placed in deep underground vaults or boreholes to reduce the level of surface wind noise in the background. The background noise levels in other parts of the spectrum are dominated by noise sources far removed from the local site. The foremost example of a source of distant noise is the 6- to 7-sec microseism peak that is present in the background at all sites worldwide; the dominant ground motion in this band is generated by processes arising in the sea, and it is observed at continental sites far removed from the coastlines. Another example of remotely generated seismic noise is the 18-sec microseism peak that is also generated in the sea, and it is also observed at interior continental sites.

The sources of the Earth's background between 20 and 40 sec are not fully understood. Locally generated wind noise dominates the background in this portion of the band in surface instruments during windy conditions. However, during calm conditions or for instruments installed at depth, the source of the lower limits of the background has remained unknown. Isolated cases of microseismic storms with energy in this portion of the band have been reported in the literature. Oliver (1962, 1963) observed a dispersive microseismic storm beginning with a 27-sec period that was detected by sensors around the world, which he established to have been generated by ocean waves impacting on the African coast bordering on the Gulf of Guiana. His conclusion was firmly supported by numerous ship's log observations of large-amplitude swell near the African coast during the time that the microseisms were observed. Haubrich *et al.* (1963) studied dispersive microseisms beginning near 25 sec generated on the southern California coastline by atmospheric storm energy propagating from the Ross Sea. They also observed secondary microseisms with periods approximately half the primary periods associated with the same storm. The current author (Holcomb, 1980) reported a storm of nondispersive microseisms with a constant period near 26 sec that were observed by stations worldwide; single-station azimuth techniques indicated that the source of these microseisms was off the southwest coast of Africa. The perplexing aspect of this storm was that the period of the microseisms was constant over several days, thereby eliminating deep water dispersion of ocean waves as the source of the narrow-band energy. Bernard and Martel (1990) confirmed the existence of this storm and presented evidence that the 26-sec microseismic energy may well have been generated by an atmospheric low-pressure center located a short distance north of the Falkland Islands.

This article presents additional information about the character of the microseismic background between 20 and 40 sec. Many years of long-period data from several stations located on five continents have been analyzed to establish the long-term behavior of the 26-sec peak. This peak persists in the Earth's microseismic background throughout the year, year after year, and is detectable anywhere in the world. The amplitude of the 26-sec peak varies with the seasons with most storm intensities peaking during the southern hemisphere winter. Observations of individual 26-sec microseismic storms at stations separated by intercontinental distances coincide, thereby indicating a singular source for the energy recorded at stations worldwide. In addition, the microseismic background between 20 and 40 sec has been scanned for

peaks in the spectra; three more extremely low-level peaks have been identified, with the possible presence of more.

Database Selection

Initially, the choice of which data to process was determined by data availability and the likelihood that the peak would be present. Based on the amplitudes of the peak reported earlier (Holcomb, 1980), stations located in Europe, Africa, the Near East, and North America would be likely candidates for study because signals were high in these areas during the previous study. It would have been prohibitive to analyze all the stations in these geographic areas due to the sheer volume of the data; at least it would have been practically impossible to process all of these data using magnetic tape. Of the stations in these areas listed, ANMO has the best station uptime record. In addition, it is very well calibrated, and it is located in a quiet continental site. Finally, the earlier study indicated that the 26-sec spectral spike was quite large in the ANMO data. Therefore, it was initially decided to analyze data from ANMO. As the analysis progressed and data processing became easier, it became evident that data from several other stations should be processed to assist in interpreting the results obtained from the ANMO data.

Figure 1 contains a map of the geographic locations of the stations whose data were processed and presented in this study. Most of them lie in the high signal parts of the world with a few from the South Pacific area to illustrate the low signal parts of the world.

Preliminary Data Processing

The results presented in this article are based on the analysis of an extremely large volume of time-series data. For instance, the results at ANMO are based on the analysis of all of the three-component, one-sample-per-second long-period (LP) data recorded at ANMO during the 15 years extending from 1980 through 1994. Similarly, the 8 years of three-component data from the 1980 through 1987 time period was processed from BCAO, CHTO, CTAO, KONO, GAC, GRFO, and NWAO. In addition, 4 years of LP data extending from 1983 through 1986 was processed from the Remote Satellite Telemetered Network (RSTN) stations RSCP, RSNT, RSNY, RSON, and RSSD. This is a total of 91 years of three-channel LP data. Processing this much data requires a highly automated data-processing algorithm in order to minimize the manual effort involved.

The raw three-component, one-sample-per-second station time-series data were read from an optical disc carousel in one-day-long segments. Following decimation by a factor of 2, these day-long segments were then broken up into approximately 42 shorter segments, each one being 4096 sec long with a 50% time overlap between segments. After removing the mean and linear trend from each segment, the fast Fourier transform (FFT) was calculated and converted to power spectral density (PSD). Each PSD segment was corrected for the combined seismometer and data-system amplitude-frequency response and was smoothed over seven spectral components in the frequency domain prior to segment averaging. Only the portion of the PSDs extending from 20 to 40 sec was retained from each segment. The decision to save only a small portion of the PSD spectrum was based on limited data storage capabilities. In retrospect, this was a bad decision, but it was necessary at the time. More data should have been saved and analyzed—particularly, shorter-period data in order to allow for a search for the second harmonic of the 26-sec energy.

PSD Segment Selection Algorithm

The raw PSD database was now ready for final processing. Up to this point, the data processing had been brute force. That is, all of the data were processed regardless of the content of the data. In order to detect the very low level 26-sec microseismic signal, it was necessary to eliminate noisy data segments (segments containing earthquakes, explosions, calibrations, wind noise, etc.) and retain only the quietest PSD segments.

A simple algorithm for selecting quiet PSD data segments to be included in the final segment-averaged PSD estimates consists of summing the PSD level over two selected bands located on either side of the anticipated 26-sec spectral peak and retaining only those segments for which this sum is the smallest. Basically, the algorithm selects segments for which the combined value of the sum of all of the PSD values contained in the FFT bins within the subbands extending from approximately 21 to approximately 24 sec, and from approximately 28 to 32 sec is the smallest served as a basis for meeting these criteria. Mathematically, this sum (S) can be expressed as

$$S = \sum_{p=20.90}^{23.95} \mathrm{PSD}(p) + \sum_{p=27.86}^{32.00} \mathrm{PSD}(p), \qquad (1)$$

where PSD(p) is the power spectral density level in the FFT bin centered about period p. Note that the sums indicated in equation (1) are not over integer indices as is normally the case in mathematical notation. Instead, the sums are denoted as being over the periods of the individual FFT bins involved. The integer FFT indices could have been used to denote the summing range, but the author believes that giving the summing range in terms of the periods involved is a much clearer method for defining the summing bands. The two noise-summing subbands bracket the portion of the PSD containing the 26-sec spectral peak, as shown in Figure 2 where they are labeled "NOISE." If the total power (S) contained in the two subbands is small, the microseismic ground motion at these periods is small, and any low-level spectrally isolated energy in the 26-sec region should not be masked by broad spectrum energy.

This segment selection criterion performed quite well

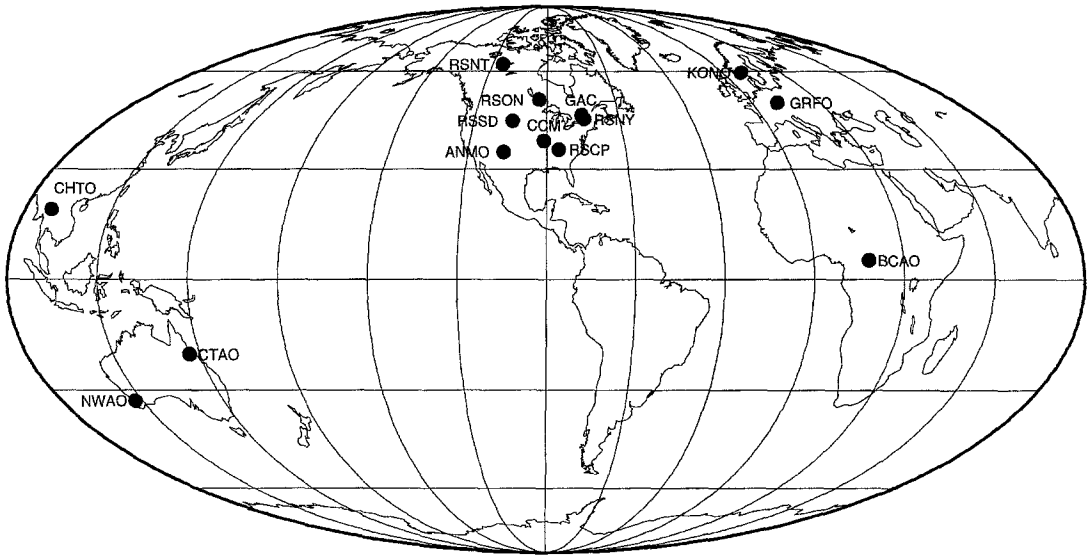

Figure 1. The geographic locations of the stations whose data were utilized to compile the results contained in this report.

for use in establishing proof of the permanent presence of the 26-sec spectral peak in the Earth's background spectra. However, it became evident that some data segments with significant 26-sec power were being discarded by the low background criterion. In addition, it was noted that some storm conditions, which were known to exist based on another systematic search of the data conducted by the author, were not being faithfully extracted by the low-noise criterion.

The apparent need was for a criterion that included information about the signal (the 26-sec peak) in addition to the information about the noise level. Therefore, a signal-to-noise ratio algorithm based on maximizing the ratio of the signal (the sum of the PSDs from 24 to 28 sec) to the previously used noise sum (equation 1) was developed and tested (see Fig. 2 for an illustration of the noise and signal bands). Mathematically, the segments for which

$$S = \frac{\sum_{p=23.95}^{27.86} \mathrm{PSD}(p)}{\sum_{p=20.90}^{23.95} \mathrm{PSD}(p) + \sum_{p=27.86}^{32.00} \mathrm{PSD}(p)}, \qquad (2)$$

the sum (S) is largest were selected for the final segment average. As might have been expected, this scheme did not discriminate against earthquakes because some earthquakes have a spectra in which this ratio is quite large. A method for eliminating event data was needed.

Finally, a successful algorithm was created by combining (by taking the product of) the criterion contained in equation (1) with the criterion in equation (2). The low-noise criterion (equation 1) assures that events were eliminated, and the signal-to-noise ratio criterion (equation 2) assures that the high-signal segments would be selected out of the remaining segments. Because we were looking for PSD segments with minimum noise, it was desirable to look for segments with minimum noise-to-signal ratio instead of maximum signal-to-noise ratio. The mathematical expression becomes

$$S = \left[\sum_{p=20.90}^{23.95} \mathrm{PSD}(p) + \sum_{p=27.86}^{32.00} \mathrm{PSD}(p) \right] \cdot \frac{\sum_{p=20.90}^{23.95} \mathrm{PSD}(p) + \sum_{p=27.86}^{32.00} \mathrm{PSD}(p)}{\sum_{p=23.95}^{27.86} \mathrm{PSD}(p)}. \qquad (3)$$

All results presented herein are based on PSD segments selected by this algorithm.

The data were processed in sequential 10-day time blocks with a 5-day overlap between blocks. Furthermore, only the 10% quietest PSD segments contained within each 10-day block as selected by the segment-selection algorithm were included in the final segment-averaged output PSD. Half of these segments were selected from the first 5 days in the block, and the rest were selected from the second half. Averaging PSD segments over many segments enhances the presence of any energy that is present in all of the PSD segments and suppresses the appearance of energy that is present in only a few of the segments; it suppresses the appearance of dispersive energy and enhances the appearance of constant period energy. Thus, the final segment-averaged PSD segment should represent energy that persists throughout the averaging period at constant frequency.

These parameters were not selected arbitrarily. The basic unit of a 5-day subblock was judged to be a lower limit

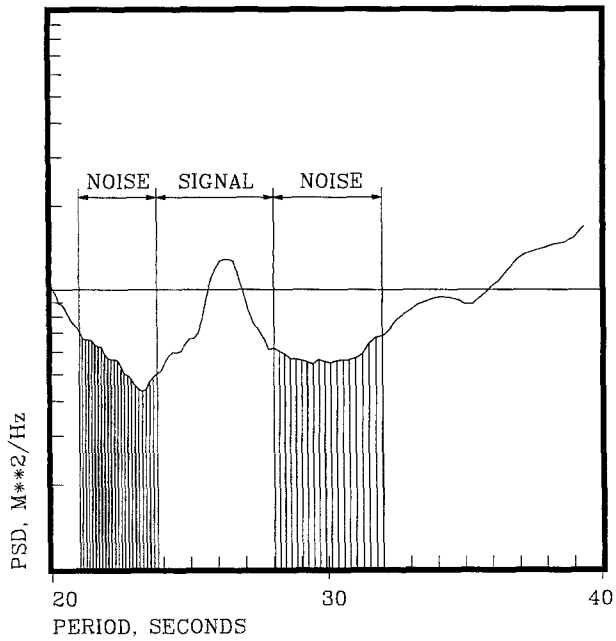

Figure 2. Definition of the noise and signal summing subbands for the segment-selection algorithm.

in hopes that the subblock would not be entirely composed of earthquake signals. During any given 5 sequential days, it is probable that at least 10% of the time will be free of such interference. The 5-day overlap between blocks provides an averaging function to smooth the data. The choice to include 10% of the data segments in the final smoothed PSD spectrum represents a trade-off between including a representative number of quiet background segments in the smoothed PSD and assuring that only low-level earth background data are included.

Long-Term Behavior of the 26-Second Peak

A power spectral density surface created by processing all of the long-period vertical data recorded at Glen Almond, Quebec, Canada, extending from 1983 through 1987, is shown in Figure 3. Each curve in this surface is the result of segment averaging several PSD segments (most curves contain the average of 43 segments if the station was operational throughout the entire 10-day period represented by each curve), and each curve extends from 20 to 40 sec on a logarithmic period scale. The individual curves are 5 days apart, and the time axis recedes into the page graduated in month tics; the southern hemisphere calendar winter–summer seasons are also approximately indicated on the time axis, and a year scale is included. The vertical axis is a linear scale with the floor of the surface representing a displacement PSD level of "approximately" 10^{-16} M^2/Hz; the floor level is "approximate" because all of the curves have been normalized to the same PSD level at 24.98 sec in order to enhance the display of the character of the surface. The PSD estimates in the PSD surfaces in Figures 3 through 5 are displacement spectra plotted on a vertical scale of 1.0×10^{-16} M^2/Hz per centimeter. Straight lines on the floor of the surface correspond to time periods during which the station was not operating.

Figure 3 is dramatic proof that the 26-sec spectral peak is a permanent feature in the Earth's microseismic background at GAC; it persists throughout the year—year after year. The amplitude of the peak varies as individual storms arise, and a definite seasonal dependence in the overall amplitude of the peak is readily observable in the PSD surface. The peak is smaller on the average during the southern hemisphere summer and significantly larger during the southern hemisphere winter.

Similarly, Figure 4 illustrates the behavior of the vertical component of the 26-sec peak at Cathedral Caves, Missouri, for the time period extending from 1990 to 1994. The overall character of this PSD surface is the same as that seen at GAC with a definite ridge in the PSD surface extending throughout the time period. The amplitude of individual storms appears to be slightly higher, but a strong seasonal dependence in their amplitude is evident at CCM just as it was at GAC. The time period shown in Figure 4 for CCM does not coincide with the time period presented in Figure 3 for GAC because the two stations were not operating during common time periods. Careful inspection of Figure 4 will reveal a second peak in the PSD surface near 30 sec, which is mostly hidden by the 26-sec ridge. This feature arises from a noise source in the Martin Marietta 24-bit digitizer that was in use at CCM during the time period extending from 1990 through early 1994; it is not due to ground motion. When this digitizer was replaced with a Quanterra Q680 digitizer early in 1994, the peak disappeared.

There are several reasons for selecting GAC and CCM as the stations to illustrate the long-term behavior of the 26-sec peak. First, both stations operated fairly continuously throughout a 5-yr time span, thereby providing a reasonably continuous time series for analysis. Second, the 26-sec ridge is more prominent at these two stations than at any other known sites. The final and most important reason for choosing these two stations is that the two stations were configured from entirely different equipment. GAC recorded the output of a KS-36000 borehole seismometer deployed at 100 m depth in a borehole on a Phoenix Data 16-bit gain ranged digitizer. The Streckeisen STS-1 sensors installed in a cave 51 m below the surface at CCM were digitized on a Martin Marietta 24-bit system during most of the time period shown in Figure 4 and on a Quanterra Q680 24-bit digital recording system the rest of the time. The uniqueness in the equipment at the two sites is important because it drastically decreases the possibility that the ridge in the PSD surfaces is an instrumentation phenomenon.

Space constraints prevent the presentation of PSD surfaces from all the stations studied. However, the results were very similar to Figures 3 and 4 for all stations in North America with the exception of RSNT and for both European stations. The PSD surface at BCAO in Africa is unique and

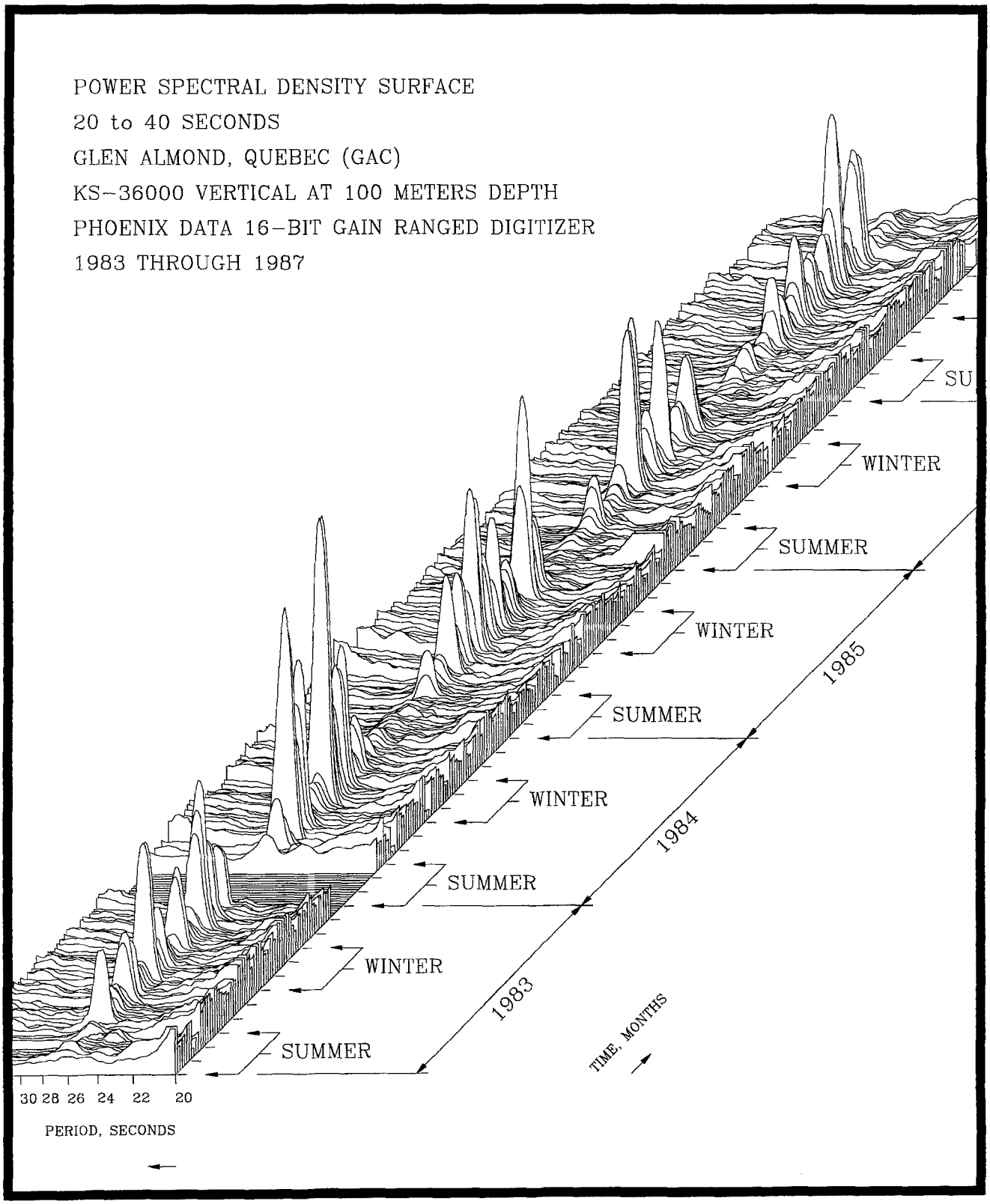

Figure 3. The PSD surface for the vertical component at GAC for 1983 through 1987.

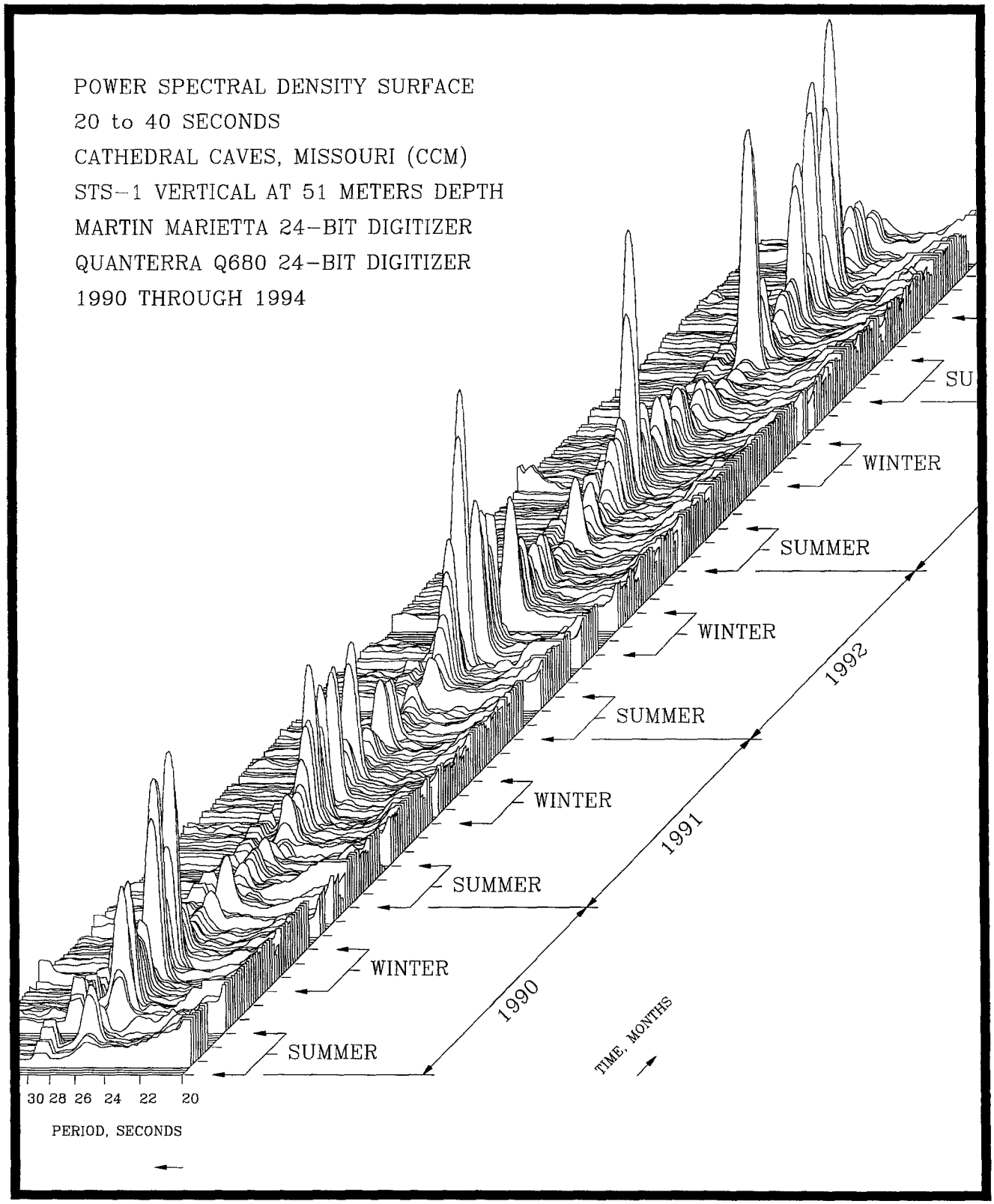

Figure 4. The PSD surface for the vertical component at CCM for 1990 through 1994.

will be discussed later in this article. Surfaces from the three Pacific stations and RSNT did not exhibit nearly as large a ridge as did GAC and CCM. As a typical example of PSD surfaces from Pacific stations, Figure 5 contains the surface from Charters Towers, Australia. At first glance, the 26-sec peak appears to be totally absent from this surface; in the next section, the presence of the 26-sec peak will be demonstrated to be present at CTAO. The lack of a prominent 26-sec peak in the PSD surfaces at Pacific stations corresponds to the results of the study of the isolated storm of 26-sec microseisms (Holcomb, 1980) in which stations in the Pacific area had drastically reduced 26-sec peak amplitudes.

The seasonal dependence of the amplitude of the 26-sec peak shown in Figures 3 and 4 and exhibited by similar PSD surfaces from ANMO, RSCP, RSNY, RSON, and RSSD provides a clue about the origin of this energy. If we assume that atmospheric weather systems are in general more energetic in the winter than in the summer (we will conveniently ignore tropical hurricanes and typhoons), and if we assume that the 26-sec energy arises either directly or indirectly from atmospheric processes, the fact that the amplitude of the peak is largest during the southern hemisphere winter indicates that the energy is generated in the southern hemisphere. This conclusion agrees with the "off the southwest coast of Africa" origin determined by the author earlier using single-station azimuth methods on storm data (Holcomb, 1980). It also agrees with the "Falkland Islands area" as a proposed source location determined by Bernard and Martel (1990).

Signal Correlation between Widely Separated Stations

There may be some readers who try to attribute the presence of the 26-sec ridge in the PSD surfaces to a multitude of hypothetical instrument problems that they believe to possibly have contaminated the data with instrument-generated signals. After all, this would not be the first time bad instrumentation has created new scientific results. Such suspicions are possible because the majority of the stations selected for this study (ANMO, CHTO, GAC, GRFO, NWAO, RSCP, RSNT, RSNY, RSON, and RSSD) utilized the same seismic sensors, Teledyne Geotech KS-36000 sensor systems installed in boreholes that are all nearly 100 m deep. Only three stations (KONO, KAAO, and CTAO) were operating the old High Gain Long Period project, 13 kg mass, Teledyne Geotech 7505A verticals and 8700C horizontals. Although KONO and KAAO detected low levels of the 26-sec ridge, none of these three stations indicated high levels of the signal. Thus, naysayers may suspect that the KS-36000 sensor generates sporadic narrow-band noise or point to the possibility of resonance phenomena in the boreholes themselves as the source of the 26-sec ridge.

The first argument against instrument generation of the unique data is the data obtained from the Strekeisen STS-1 installation 51 m below the surface at CCM as recorded on a Martin Marietta 24-bit digitizer (data recorded late in 1994 was digitized on a Quanterra Q680 digitizer); these data are shown in Figure 4. This is an example of a second manufacturer's seismic sensor system installed in a unique environment recorded on a different digital recording system that produces one of the best examples of the 26-sec ridge recorded at any of the sites. It would seem impossible that equipment can be producing the data.

Nevertheless, the author believes that it is important to demonstrate the degree of signal correlation between widely separated stations and to invoke the argument that the simultaneity of signals observed at several sites rules out instrumentation as a source of the signal because it is unlikely that the instrumentation could generate simultaneous signals at widely separated sites. In this case, the term signal refers to the amplitude of the 26-sec peak as a function of time. The PSD surfaces in Figures 3 through 5 contain many 5-yr-long PSD amplitude time series sampled at a 5-days-per-sample interval; the time series whose points pass through the peaks in the PSD surfaces will be the signal to be analyzed. First, the excellent signal correlation between the stations in North America will be illustrated; then correlation between North American and European stations will be shown.

Figure 6 presents the unnormalized vertical 26.09-sec FFT bin time series from ANMO, GAC, RSSD, RSCP, RSNY, RSON, and RSNT for the years extending from 1983 through 1986. This is essentially all of the data available from the five RSTN stations because that network was only operational during that time period. Furthermore, the largest PSD level in each series has been normalized to the same value for all four stations in order to adjust for variations in path attenuation effects. The vertical scale in the figure has not been labeled because the emphasis in the figure is not on the absolute amplitude at each site; we are interested in the relative shape of the time series and the coincidence of peaks therein.

The time series in the figure reveal that there is a high degree of visual correlation between the peaks in the signals recorded at all of these stations except for RSNT. Note the remarkable correspondence between the relative levels of time-coincident peaks at all stations. Remember that these stations are distributed throughout the northern portion of North America; most of them are separated by hundreds of kilometers. Table 1 contains a distance separation matrix for the seven stations involved in this interstation signal correlation study. The high degree of similarity of the signals recorded at these stations is strong evidence that the 26-sec signal is not a result of instrumentation problems. It is incomprehensible that stations operated by three different agencies separated by hundreds to thousands of kilometers and recording data from two unique seismic sensor systems on three unique digital data recording systems could all produce simultaneously erroneous data. The 26-sec data recorded at these widely separated stations must be a result of

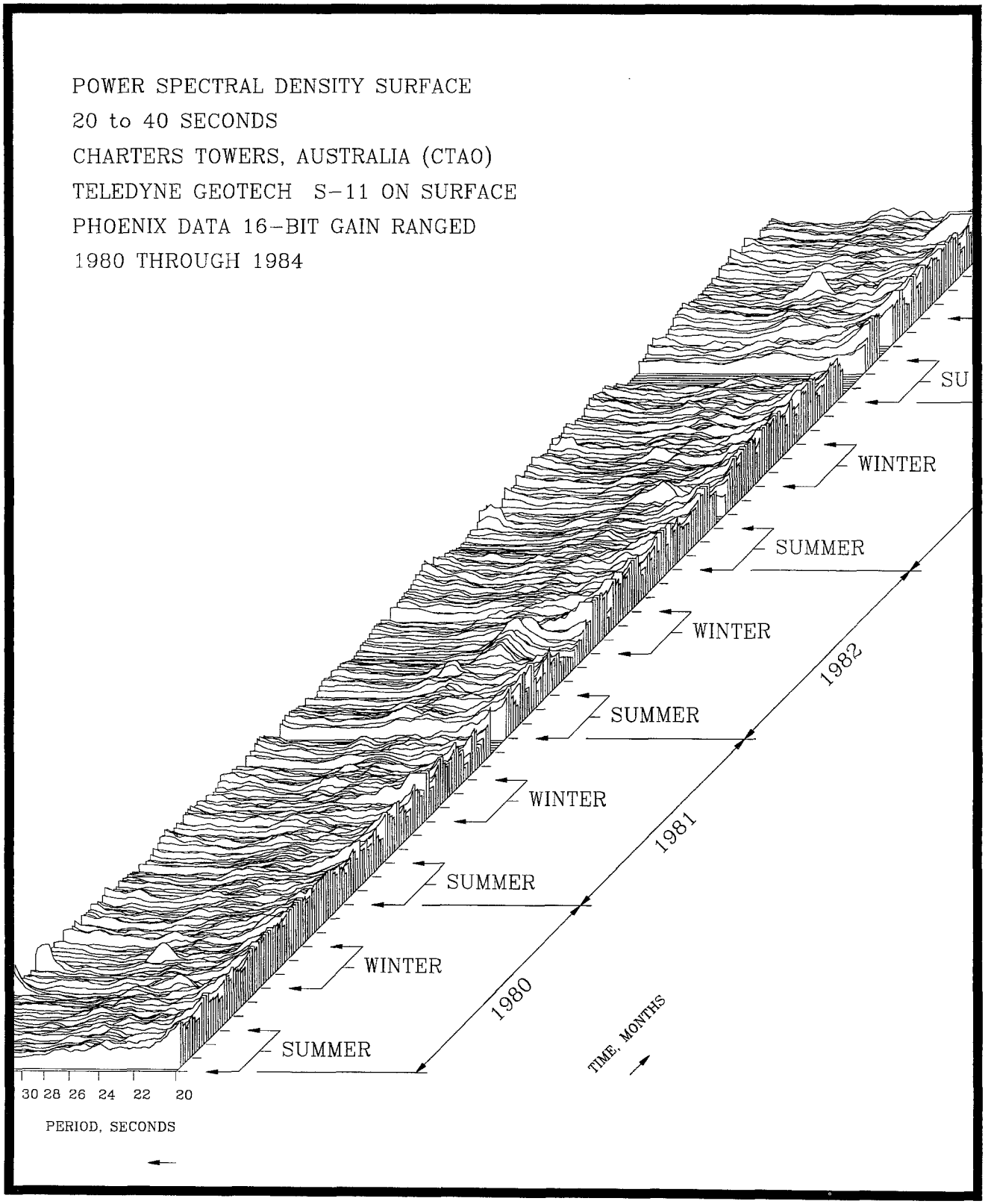

Figure 5. The PSD surface for the vertical component at CTAO for 1980 through 1984.

an actual signal arising from a common source remote from all of the stations, which generates propagating ground motion that is recorded nearly simultaneously at all sites.

Visual correlation between the vertical 26.09-sec FFT bin time series between ANMO in North America and stations in Europe and Africa for the years extending from 1984 through 1987 is shown in Figure 7. Unfortunately, BCAO was not operational some of the time, and it was quite noisy much of the time, but there are enough data to support the argument that the 26.09-sec FFT bin time series correlates over intercontinental distances. The correlation between the larger peaks in these time series is readily evident in the figures particularly between ANMO and GRFO, and at times with BCAO, but the correlation between the smaller peaks does not appear to be as high as it was for stations within North America.

The conventional linear correlation coefficients (see Press *et al.*, 1986, p. 484) between the vertical time series in Figure 6 for stations in North America are tabulated in Table 2. The degree of correlation between most of the widely separated stations is truly remarkable. This becomes even more evident if we consider the intercomponent correlation between the vertical and east components at ANMO and GAC. The correlation coefficients between the ANMO

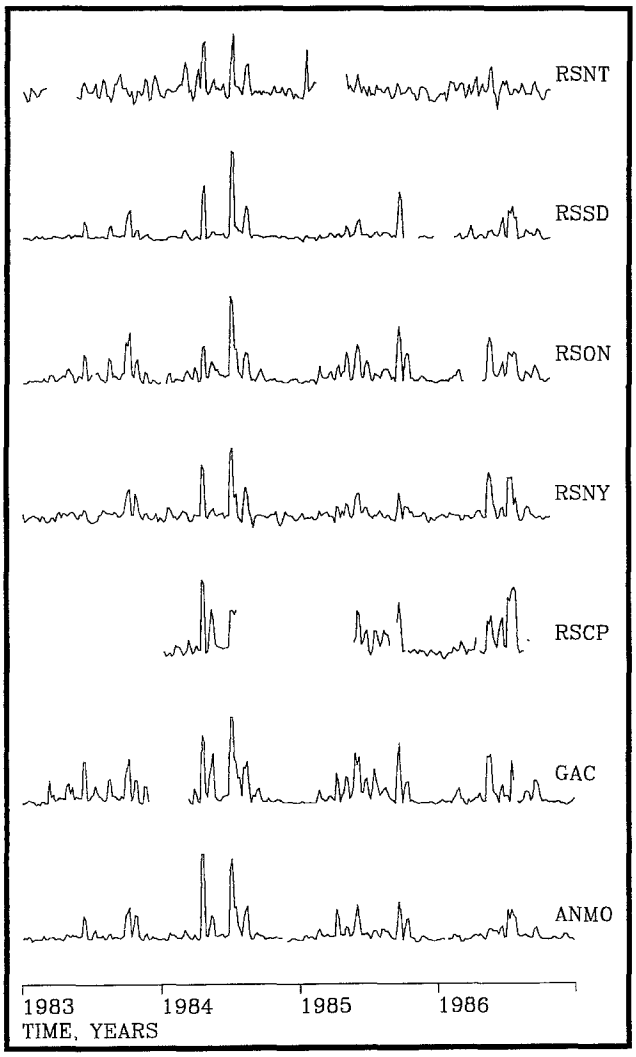

Figure 6. Correlation of the time series of the 26.09-sec FFT bin from seven stations in North America.

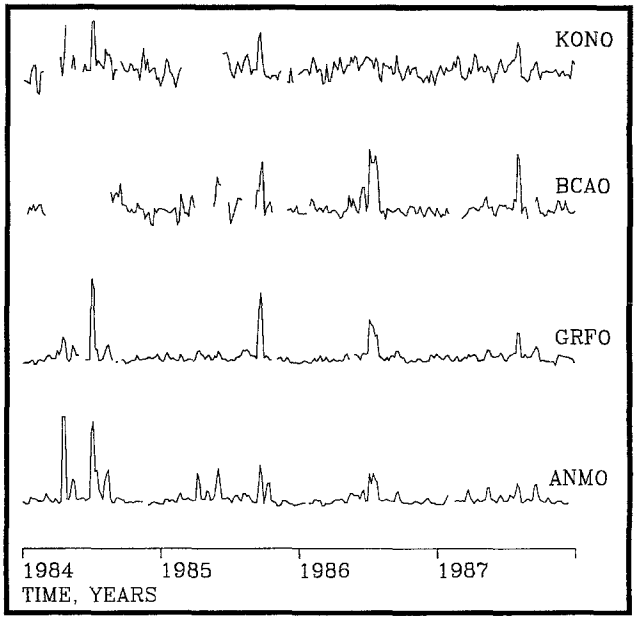

Figure 7. Correlation of the time series of the 26.09-sec FFT bin at intercontinental distances.

Table 1

Station-Separation-Distance Matrix for the Seven Stations Utilized in the North American Interstation Signal Correlation Study (separation distances are in kilometers)

	ANMO	GAC	RSCP	RSNT	RSNY	RSON	RSSD
ANMO	0	2859	1888	3110	2906	2023	1039
GAC	2859	0	1315	3082	148	1430	2242
RSCP	1888	1315	0	3494	1282	1668	1767
RSNT	3110	3082	3494	0	3228	1842	2151
RSNY	2906	148	1282	3228	0	1559	2333
RSON	2023	1430	1668	1842	1559	0	1068
RSSD	1039	2242	1767	2151	2333	1068	0

Table 2

Interstation Linear Correlation Coefficients for the Vertical 26.09-sec FFT Bin Time Series from Several Widely Separated Stations in North America

	ANMO	GAC	RSCP	RSNT	RSNY	RSON	RSSD
ANMO		0.93	0.95	0.34	0.90	0.96	0.96
GAC	0.93		0.96	0.24	0.91	0.98	0.97
RSCP	0.95	0.96		0.23	0.95	0.97	0.96
RSNT	0.34	0.24	0.23		0.26	0.21	0.32
RSNY	0.90	0.91	0.95	0.26		0.92	0.91
RSON	0.96	0.98	0.97	0.21	0.92		0.98
RSSD	0.96	0.97	0.96	0.32	0.91	0.98	

vertical and ANMO east time series is 0.93, and the coefficient between the same two components at GAC is 0.96. These intercomponent values are approximately equal to most of the interstation correlation coefficients for the vertical 26.09-sec PSD time series in Table 2. Since the same source undoubtedly generates the 26-sec signal on both the vertical and horizontal components at a given site, these data are indicative of the lower limits of the signal-resolution ability of the signal-processing algorithms. Within the limits of the algorithm's signal-extraction ability, the signals recorded at all but one of the North American sites are the same signals arising from a common source remote from all of the station locations.

Signal-to-Noise Ratios

The signal-to-noise ratios (SNRs) of the 26-sec peak averaged over time provides a quantitative measure of the prominence of the ridge in the PSD surfaces at the stations. Equation (4) defines the average noise level that is taken to be the average of the PSD level of the seven FFT bins in the 24- to 25-sec band averaged over M PSD segments, where M is the total number of PSD segments available for each station in the number of years indicated in Table 3. This band was chosen somewhat arbitrarily, but it should provide a good estimate of the out-of-band noise near the 26-sec signal band:

$$N = \frac{1}{M}\sum_{n=1}^{M}\left[\frac{1}{7}\sum_{p=24.09}^{24.98}\mathrm{PSD}_n(p)\right]. \tag{4}$$

The signal as defined by equation (5) is the average PSD level of the four FFT bins at the top of the peak averaged over M PSD segments. The average SNR is the ratio of equation (5) to equation (4), and the results for all of the stations studied are shown in Table 3. Notice that GAC and CCM have by far the highest average SNR values and that all of the remaining stations in North America with the exception of RSNT have SNRs near 2.0. The averages for BCAO, GRFO, and KONO are slightly greater than 1, and the SNRs for the Pacific stations including RSNT are less than or equal to 1.0.

$$S = \frac{1}{M}\sum_{n=1}^{M}\left[\frac{1}{4}\sum_{p=25.92}^{26.43}\mathrm{PSD}_n(p)\right]. \tag{5}$$

Peak-Detection Algorithm

The PSD surfaces in Figures 3 and 4 are adequate to reveal the continuous presence of the 26-sec peak in the Earth background. In addition, careful inspection of the two figures reveals that a second peak may exist in the background near 24 sec, especially at GAC. This raises the question of whether or not additional invisible spectral structure may be present in the PSD surfaces. To answer this question, a software peak-detection algorithm was formulated and implemented to analyze each PSD segment data for "significant peaks" and to tabulate the number of peaks found at each period.

Table 3
Tabulation of the Vertical 26-sec Signal-to-Noise Ratios

Station Code	Number of Years	SNR Average
ANMO	14	1.7
BCAO	7	1.6
CCM	5	3.6
CHTO	8	0.7
CTAO	8	0.8
GAC	5	3.2
GRFO	8	1.4
KONO	8	1.1
NWAO	8	0.2
RSCP	4	2.2
RSNT	4	1.0
RSNY	4	1.7
RSON	4	2.9
RSSD	4	1.9

The algorithm was essentially designed to duplicate in a quantitative manner the action of the eye in a qualitative manner; it was designed to detect the most significant peaks in the PSDs and to reject the lesser peaks. Because many of the major peaks in the PSD figures are shaped somewhat like parabolas, the peak-detection algorithm was based on determining how well a least-squares-fitted parabola approximated short sections of the actual PSD data.

A visual study of the data indicated that many of the prominent peaks were approximately 2 sec wide at the base (the point at which the peak merged with the apparent background); therefore, 2-sec-wide parabolas were chosen as the appropriate width. A 2-sec-wide parabola centered on every FFT bin in each PSD segment was least-squares fitted to the PSD values within the 2-sec band in the period domain. While fits near the short-period end of the PSD segments contained many more fitted points than those near the long-period end, the process appeared to function quite well. The criteria for declaring a peak or rejecting the fit was that the coefficient of the second-order term must be less than a threshold value (-0.1). This combination of parameters produced a fitting algorithm that picked peaks that projected roughly the 95% confidence interval above the surrounding apparent background.

Figure 8 contains an example of the performance of the peak-detection algorithm. In this figure, the least-squares-fitted parabolas have been offset above the PSD data to increase their visibility. As shown in Figure 8, the peak-detection algorithm found peaks centered at 23.81, 26.77, and 33.03 sec. One might argue that another peak is evident in this figure somewhere around 30 sec. However, the second-order coefficient for this peak was equal to -0.1, not less than -0.1; this potential peak was just barely rejected by the algorithm as a nonpeak.

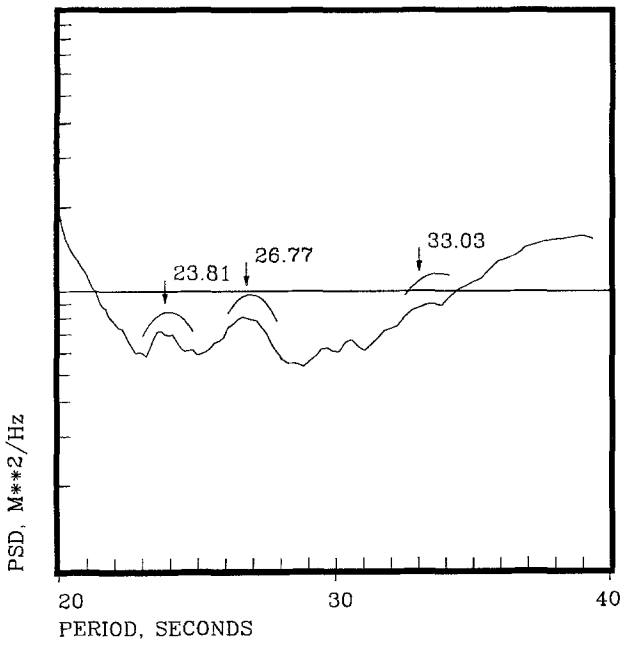

Figure 8. Example of the parabolic peak-picking algorithm performance.

Peak-Detection Histograms—Three New Peaks

The results of applying the peak-detection algorithm to the 5-yr PSD surface for GAC in Figure 3 are shown in the peak histogram of Figure 9 that summarizes the total number of peaks detected with the parabola centered on each FFT bin. As should be expected, there are a large number of peak detections near 26 sec corresponding to the 26-sec ridge of Figure 3. There is also evidence for the existence of additional peaks in this histogram; the FFT bins associated with the potential new peaks have been grouped between the arrows in the figure and are numbered groups 1, 3, and 4. The peak picks contained in FFT bins for periods shorter than those in group 1 and longer than those in group 4 will be ignored; the peak-detection algorithm could not reliably pick peaks in this portion of the spectrum because only the portion of the PSD spectrum extending from 20 to 40 sec was saved. The number of detected peaks in the three new groups appears to be small because the 26-sec ridge dominates; their existence will be confirmed by data from other sites.

The histogram for CTAO in Figure 10 differs significantly from the histogram from GAC; the peak picks in groups 1, 3, and 4 appear to be much more prominent because the number of peak picks in the 26-sec group are much less. The peak detector confirms the presence of the 26-sec peak in the CTAO PSD surface, even though the eye may not detect it. Notice that at CTAO there are more peak detections in group 1 than there are for the 26-sec peak in group 2. The peak detector confirms what the critical eye tends to see in Figure 5; that is, there appears to be a peak in the CTAO PSD surface just above 24 sec. This histogram is typical of the histograms for the other three stations in the Pacific region

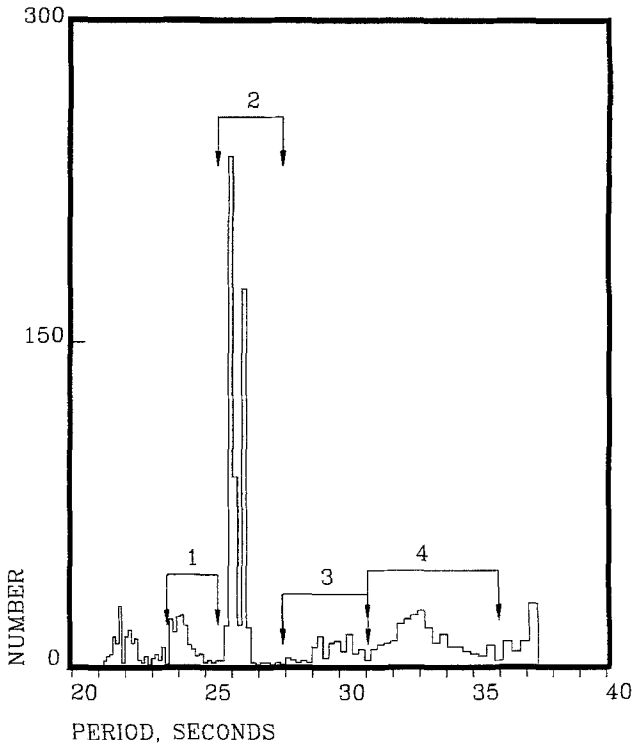

Figure 9. Histogram of the peaks detected in the PSD surface for the vertical component at GAC during 1983 through 1987.

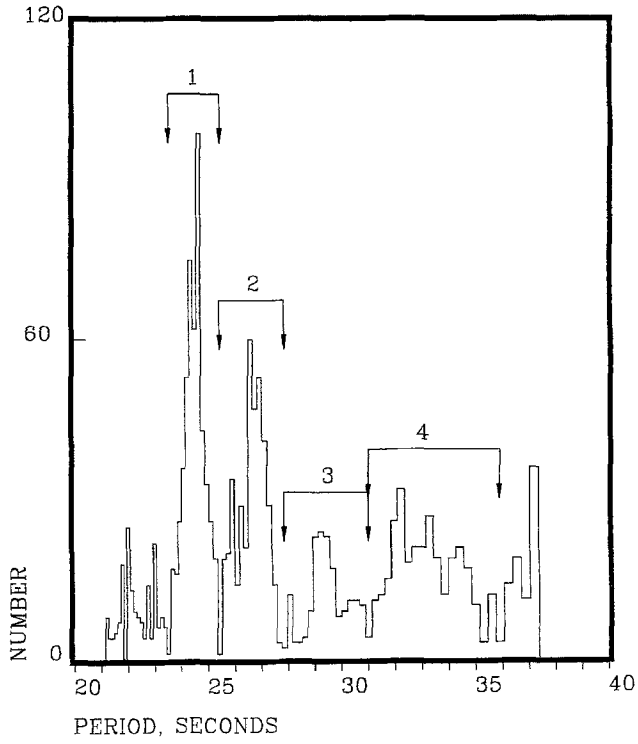

Figure 10. Histogram of the peaks detected in the PSD surface for the vertical component at CTAO during 1980 though 1987.

(CHTO, NWAO, and RSNT): All three contain significantly reduced numbers of peaks in group 2, and more peaks are detected in group 1 than are found in group 2.

The remarkable feature of all of the histograms from stations in North America, Europe, and the Pacific is that the peaks in all of these histograms can be grouped in the same four basic groups shown in Figures 9 and 10. The spectral structure in the Earth's background at all of these sites is the same! Figure 11 contains a summary of all of the peaks detected at ANMO, CHTO, CTAO, GRFO, KONO, NWAO, GAC, RSCP, RSNT, RSNY, RSON, and RSSD; note the well-defined minimums in the peak counts corresponding to the dividing boundaries between adjacent groups.

Prior to this study, the 26-sec peak was known to exist only in storms. Its existence in storms led to this study of very low levels of the 26-sec peak in an attempt to show that this peak persists throughout time. This in turn led to the discovery of the existence of three new low-level peaks in the vicinity of 26 sec. Next, it might be asked, do storms ever occur at any of the newly identified peak periods? In the author's opinion, the answer is that they probably do. Isolated examples of possible storms in group 1 have been observed by the author during this survey over the past years, but before the histograms were constructed, their possible significance had not been apparent. The PSD surface from CTAO in Figure 5 shows somewhat increased levels in group 1 in June and July of 1982 that may be indicative of group 1 storm activity. This question should be the subject of future investigations.

The critical reader may notice that the peak in group 2 of the histogram for GAC in Figure 9 appears to be split and may argue that group 2 should be composed of two groups; the 26-sec peak really appears to be two closely spaced peaks. Although not shown, group 2 also appears to be split in exactly the same manner in the histograms from RSCP, RSNY, RSON, RSSD, and CCM. There are also indications of two closely spaced peaks in the group 2 histograms at GRFO and KONO. The summary histogram in Figure 11 also shows the possibility of two peaks in group two; this is the result of the influence of the histogram data from CCM, GRFO, KONO, RSCP, RSNT, RSNY, RSON, and RSSD on the combined histogram. In contrast, the 14-yr histogram at ANMO does not show evidence of two distinct peaks. The author believes that the jury is still out on the detailed spectral structure in group 2. The apparent splitting of the 26-sec peak may be real or may be an artifact of the data-processing algorithms; this question will be the subject of future investigations.

The nature of the 26-sec peak in the histogram of Figure 12 at BCAO is quite unique. There is no question that there are two major peaks in group 2; one occurs near 25.73 sec, and the second is near 27.31 sec. The origin of these two peaks is certainly not understood. This is the only station at which this spectral structure was observed in the microseis-

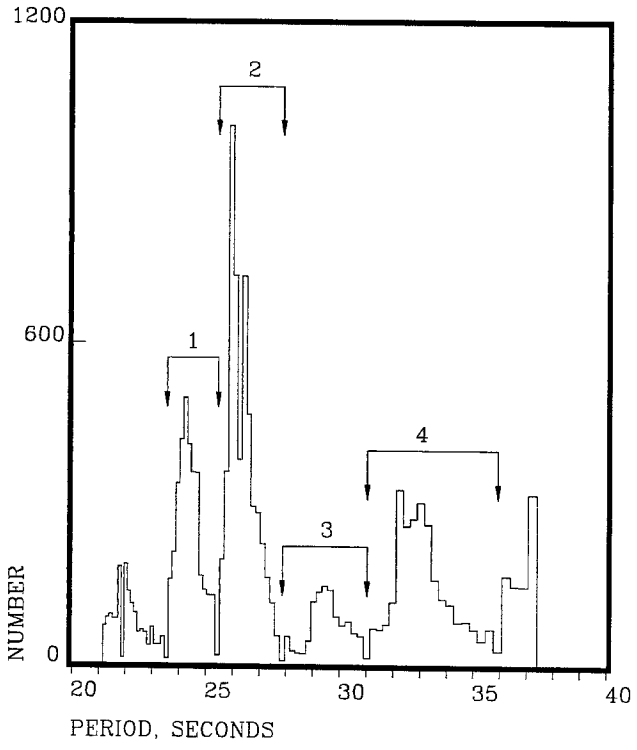

Figure 11. Histogram summarizing all of the peaks detected in the vertical PSD surfaces at ANMO, CHTO, CTAO, GRFO, KONO, NWAO, GAC, CCM, RSCP, RSNT, RSNY, RSON, and RSSD. This figure contains approximately 83 station years of data.

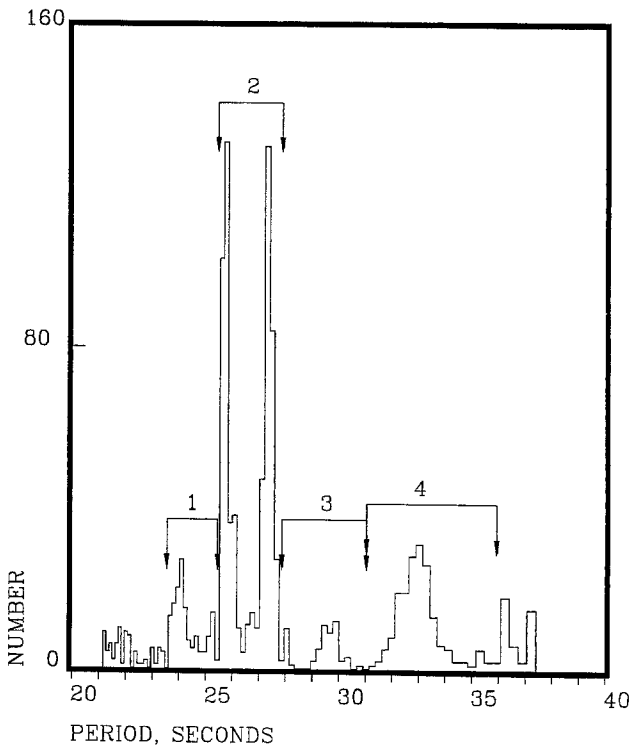

Figure 12. Histogram of the peaks detected in the PSD surface for the vertical component at BCAO during 1980 through 1987.

mic background, so it is conceivable that the phenomena arises in an instrumentation malfunction at BCAO. On the other hand, preliminary azimuth calculations indicate that the energy in the two peaks arrives at BCAO from two unique directions. Several new broadband low-noise stations have recently been installed in Africa, and more are planned in the future. Further analysis of data from additional stations in the area should assist in resolving the true nature of the microseismic background near 26 sec in that part of the world.

Geophysical Filtering—A Proposed Source Mechanism

The combination of the atmosphere with the ocean and with the Earth is a very complex geophysical system in which there are a myriad of potential mechanisms for explaining the presence of the 26-sec peak. It is difficult to pin down the specific source of the 26-sec energy based on the evidence on hand. However, it should be possible to make some reasonable observations. First, let us summarize what is known based on the author's earlier work (Holcomb, 1980), Bernard's observations (Bernard and Martel, 1990), and the present results.

- The peak period is constant at all stations.
- The peak period is the same at all stations.
- The peak is very narrow band at all stations.
- The peak persists throughout time at all stations.
- The amplitude of the peak varies over a wide range.
- The source region does not change with time.
- The peak amplitude is large in North America, Europe, the Middle East, and Africa.
- The peak amplitude is small in the Pacific region and South America.
- The peak amplitude is seasonally dependent.
- Storms are coincident at stations separated on an intercontinental scale.

The fact that the amplitude of the 26-sec peak varies over a wide range in individual storms and that the amplitude of individual storms is seasonally dependent suggests that the originating source of this energy arises in the Earth's atmosphere. The fact that the peak is very narrow band tends to argue against atmosphere as being the sole source of the peak because atmospheric processes are probably rather broadband. The presence of a geophysical filter appears to be necessary in order to produce the phenomenon.

For the purposes of discussion, express the experimentally measured power spectra, $X(\omega)$, in the form of a linear-system power transfer function as follows (see Bâth (1974), Chap. 6, for notation):

$$X(\omega) = S(\omega) \cdot H(\omega) \cdot R(\omega), \tag{6}$$

where $S(\omega)$ is the power spectral density of the source, $H(\omega)$ is the source-to-station propagation transfer function describing the effects of propagating from the source to the seismic station, and $R(\omega)$ is the seismometer site transfer function.

First, the term $R(\omega)$ may be thought of as being composed of two subtransfer functions such as

$$R(\omega) = A(\omega) \cdot C(\omega), \tag{7}$$

where $A(\omega)$ is the seismometer transfer function and $C(\omega)$ denotes the effects of crustal reverberation or resonances in the vicinity of the station. The instrument transfer functions are known from calibration data and have been removed from the PSD data in this report, so $A(\omega)$ is not a factor. The crustal reverberation response $C(\omega)$ can sometimes be quite large, but it is apparently not responsible for generating the 26-sec energy because the period of the peak in the PSD is the same at all stations. One would expect receiving site crustal effects to be unique when the receiving sites are separated on a worldwide scale. Therefore, we can eliminate $C(\omega)$ from consideration; $R(\omega)$ filtering is not the source of the 26-sec peak.

Similarly, the source-to-station propagation transfer function, $H(\omega)$, can be ruled out as a source of filtering action with the same type of argument because the paths of propagation are so radically different for the various stations that many unique paths are traveled with identical peak characteristics in the PSDs at all stations.

Therefore, we are left with the source function $S(\omega)$ as being the most probable source of filtering action. Assuming that the source energy originally arises in the atmosphere, is first coupled to the ocean, and then is converted to seismic waves in the Earth, $S(\omega)$ may be thought of as being expanded as

$$S(\omega) = E(\omega) \cdot O(\omega) \cdot C(\omega) \cdot D(\omega,\theta), \tag{8}$$

where $E(\omega)$ is the spectra of the atmospheric energy source, $O(\omega)$ represents the transfer function of the ocean, $C(\omega)$ indicates the effects of crustal reverberations or resonances in the vicinity of the source, and $D(\omega, \theta)$ is a source direction factor with θ denoting the direction of propagation from the source. The nonsymmetrical geographical variation in the amplitude of the 26-sec peak about the suspected source region (Holcomb, 1980) implies that $D(\omega, \theta)$ is not equal to 1. There must be a strong azimuthal dependence of the energy radiated from the source. As mentioned earlier, the seasonal dependence of the 26-sec peak argues for an atmospheric source for the energy, but atmospheric processes are not likely to directly generate narrow-band spectra. Therefore, $E(\omega)$ is probably the source of the energy but not its narrow-band character.

We are left with the combined response of the ocean and the Earth in the source region $O(\omega) \cdot C(\omega)$ as the most likely source of the filtering action. There does not appear to be any currently known process in the geophysical world

that could act as a filter to generate narrow-band constant-period energy on a continuous basis. In the oceans, deep water dispersion of broadband wave energy generated by atmospheric storms at sea can create narrow-band microseisms but not with constant period except under highly specialized conditions. The author proposes that the filtering action occurs in the form of a resonance process in the ocean near the source, or in the Earth near the source, or in the combined ocean–Earth system near the source. An example of such a resonant process might be a seiche in a body of water of the proper size excited by atmospheric storms. Resonant processes tend to be narrow band with the resonant frequency being determined by the mechanical dimensions and properties of the system involved. A detailed model of this process must await additional data and further insight.

Conclusions

The original object of this study was to establish that the author's earlier report of a spectral line in the Earth's background spectra near 26 sec (Holcomb, 1980) was not an isolated example, but rather that a spectral peak exists near 26 sec on a continuous basis.

This objective has been achieved, and additional information about the nature of the spectra of the microseismic background between 20 and 40 sec has emerged as a by-product of the effort. There is a prominent peak near 26 sec that is readily evident in the Earth background spectra throughout North America, Europe, and Africa. The presence of this peak is essentially continuous with time at all sites throughout this area, and the period of this peak is absolutely constant (within the resolution limits of the analysis) with time at all sites. With the exception of BCAO, the period of this peak is the same at all sites throughout both the high- and low-signal amplitude portions of the world. The size of the peak is drastically reduced at sites near and in the Pacific Ocean, but the peak is resolvable on a continuous basis at all stations studied. The amplitude of the 26-sec peak varies with the seasons; the highest amplitudes occur during the southern hemisphere winter, thereby implying that the energy is being generated in the southern hemisphere.

The presence of at least three additional new peaks in the background between 20 and 40 sec has been identified by this study. Despite the fact that these new peaks are very low level, they are detectable in the background worldwide. Thus, the lower limits of the background between 20 and 40 sec appears to be primarily composed of power that appears in distinct bands instead of in a continuum as most might expect. The geographic locations of the sources of the three new peaks is unknown and will probably be very difficult to determine because of the extremely low amplitudes.

Acknowledgments

The author appreciates the assistance of Jim Redmond of Diversified Technology, who mounted and initiated the overnight processing of literally hundreds of magnetic tapes during the early stages of this study. Bob Woodward and Scott Halbert at ASL assisted the author in solving several data-processing roadblocks. Stuart Koyanagi and Pam Benfield at NEIC were instrumental in recovering from a severe file-corruption problem that was created when ASL switched from a VAX to a SUN-based computing network. A special thank you to the many personnel responsible for the design and installation of the seismological stations, to the personnel who dutifully operate and maintain these stations throughout the years, and to the personnel responsible for the quality control and archiving of the data. Without their often-ignored dedication, studies of Earth-motion phenomena would be impossible.

References

Båth, M. (1974). *Spectral Analysis in Geophysics,* Elsevier, Amsterdam.

Bernard, P. and L. Martel (1990). A possible origin of 26 s microseisms, *Phys. Earth Planet. Interiors* **63,** 229–231.

Haubrich, R. A., W. H. Munk, and F. E. Snodgrass (1963). Comparative spectra of microseisms and swell, *Bull. Seism. Soc. Am.* **53,** 27–37.

Holcomb, L. G. (1980). Microseisms: a twenty-six-second spectral line in long-period Earth motion, *Bull. Seism. Soc. Am.* **70,** 1055–1070.

Oliver, J. (1962). A worldwide storm of microseisms with period of about 27 seconds, *Bull. Seism. Soc. Am.* **52,** 507–517.

Oliver, J. (1963). Additional evidence relating to "a worldwide storm of microseisms with period of about 27 seconds," *Bull. Seism. Soc. Am.* **53,** 681–685.

Press, W. H., B. P. Flannery, S. A. Teukolski, and W. T. Vetterling (1986). *Numerical Recipes,* Cambridge U Press, New York.

Albuquerque Seismological Laboratory
U.S. Geological Survey
Building 10002, KAFB East
Albuquerque, New Mexico 87115
E-mail: gary@asl.cr.usgs.gov

Manuscript received 29 May 1997.